

Dynamical transitions in aperiodically kicked tight-binding models

Vikram Ravindranath*

*Department of Physics and Astronomy, CUNY College of Staten Island, Staten Island, NY 10314,
Physics Program, The Graduate Center, CUNY, New York, NY 10016.*

M. S. Santhanam†

Indian Institute of Science Education and Research, Dr. Homi Bhabha Road, Pune 411 008, India.

If a localized quantum state in a tight-binding model with structural aperiodicity is subject to noisy evolution, then it is generally expected to result in diffusion and delocalization. In this work, it is shown that the localized phase of the kicked Aubry-André-Harper (AAH) model is robust to the effects of noisy evolution, for long times, provided that some kick is delivered once every time period. However, if strong noisy perturbations are applied by randomly missing kicks, a sharp dynamical transition from a ballistic growth phase at initial times to a diffusive growth phase for longer times is observed. Such sharp transitions are seen even in translationally invariant models. These transitions are related to the existence of flat bands, and using a 2-band model we obtain analytical support for these observations. The diffusive evolution at long times has a mechanism similar to that of a random walk. The time scale at which the sharp transition takes place is related to the characteristics of noise. Remarkably, the wavepacket evolution scales with the noise parameters. Further, using kick sequence modulated by a ‘coin toss’, it is argued that the correlations in the noise are crucial to the observed sharp transitions.

I. INTRODUCTION

It is by now well established through theoretical studies and experiments that periodic forcing imparted to quantum systems can lead to novel states of matter that did not exist in its time-independent counterpart [1–4]. For the periodically driven Hamiltonian systems, Floquet states represent the natural generalization of the stationary eigenstates for time-independent systems. These states are interesting objects of study because they can exhibit more complex dynamics and allow more control through external driving in comparison to their static counterparts. Many phenomena in static systems such as the topology of band structures [5] and transport properties [6, 7] can be tuned by an appropriate driving mechanism. A class of such techniques now known as Floquet engineering [1, 8, 9] attempt to create novel Floquet states with desired topological properties [10, 11] by designing an effective time-independent Hamiltonian for the driven systems. In the last decade, experiments have implemented a variety of approaches based on such Floquet manipulations – effective Hofstadter Hamiltonian using cold atoms in optical lattices [12], control over direction and interference of phonon flow in 2D array of trapped ions [13], the implementation of Haldane model in ultracold fermions to realize topological insulators [14] and control over heating due to periodic drive in pre-thermal phase of Bose-Hubbard system [15]. Recently, principles of Floquet engineering have been extended to quantum dissipative systems as well thus providing a handle to understand non-equilibrium steady states [16].

In this broader context, of particular interest in a variety of condensed matter systems is the observation of quantum localization of eigenstates in time-independent systems and of Floquet states in time-dependent systems [17, 18]. Quantum kicked rotor, representing the dynamics of a periodically kicked pendulum, is a well studied example of a classically non-integrable system. The classical limit of kicked rotor, for strong kick strengths, displays chaotic dynamics and energy diffusion [19]. The corresponding quantum system exhibits stark differences from classical regime, and localization of all its Floquet states is a notable feature amongst them [19]. The quantum kicked rotor has been mapped to the Anderson tight binding model for a particle in a crystalline lattice with random on-site potentials [20]. These connections have been experimentally explored using cold atoms in optical lattices over the last three decades [21]. Thus, far from being theoretical constructs, tight-binding models have become popular partly owing to their ease of experimental realisation in optical lattices [22].

Floquet systems are characterised by periodic driving with periodicity T such that drive term $f(t)$ satisfies $f(t + T) = f(t)$. In typical experimental situations, there are bound to be imperfections and this provides a motivation to consider noise in T and other parameters related to the drive term. More importantly, there is a strong possibility of novel effects arising due to presence of aperiodicity in Floquet systems. For instance, all the Floquet states of the quantum kicked rotor in one and two dimensions are localized, and do not display a localization to delocalization transition. However, noisy kick sequences can induce such a transition. If the kick period is perturbed by stationary noise, dynamical localization is destroyed through an exponentially decaying decoherence process resulting in a delocalized phase. This aspect has been extensively studied in kicked rotors

* vravindranath@gradcenter.cuny.edu

† santh@iiserpune.ac.in

[23–25]. Interestingly, recent theoretical proposals [26] and experimental realizations show that the localization to delocalization transition can be non-exponential upon introducing nonstationary noise in the kicking sequence [27]. In general, without noisy kicks, the localization to delocalization transition is absent in the one-dimensional kicked rotor.

Though the localization-delocalization transition is absent in kicked rotors (and also in Anderson model) of one and two dimensions, it is known that quasi-periodic lattice models such as the Aubry-André model do display such a transition even in one dimension [28]. Depending on the presence or absence of interactions and the parametric regime under consideration, particular effects of *periodically* driving the Aubry-André system vary from preserving the localization transition [29], inducing delocalization [30] to the appearance of a Griffiths-like phase manifesting as slow dynamical spreading [31]. Generally, the phase boundaries depend on the amplitude and frequency of the driving field [6].

Then, the question arises as to how such systems with built-in structural aperiodicity react to noisy driving fields or kick sequences imparted to them. In this paper, the kicked Aubry-André system, belonging to a class of aperiodic lattice models, is studied to examine the effects of noisy kicks in which noise manipulates the periodic kick sequence in three different ways. In this context, it is of interest to distinguish between milder forms of noisy kicks in which only the amplitude of kicks are modulated as opposed to the stronger forms in which entire kicks can be missed. If a tight-binding model that supports a localized regime is *irregularly* kicked, we generally expect to observe a localization to delocalization transition analogous to the behaviour of the quantum kicked rotors under milder forms of noisy kicks [23, 26, 27]. For instance, such a scenario also unfolds in the case of Floquet topological chains treated analytically using the Floquet superoperator formalism [32]. In this case, strictly periodic kicks preserve topologically protected end states, and noisy kicks lead to a decay of these topologically protected modes. It is also known that localized regime in the kicked Aubry-André model survives even if a milder form of noise is present [33].

In contrast, in this study, the focus is on the effects of stronger forms of noisy kick sequences imparted to an initially localized state. It is shown that a dynamical transition from ballistic to diffusive growth results. The characteristics of this transition, whether smooth or abrupt, and the timescale at which this transition takes place depend on the noise properties. Remarkably, by tuning the characteristics of noise, the timescale for the transition from ballistic to diffusive can be tuned as well. It is shown that the wavepacket growth quantified by its second moment scales with a noise parameter. Rest of the article is structured as follows – in sections II and III, we describe the AAH model and noisy driving protocols, in sections IV and V the simulation results are presented, and in sections VI and VII the results are extended to

translationally invariant models and analytical support is provided for the main features of the results. Section VIII provides a brief summary of the results.

II. DYNAMICAL PROPERTIES

A. Model

The Hamiltonian of the model considered in this work is given by

$$H = H_0 + V \sum_n \delta(t - T_n) \sum_{i=1}^L V_i c_i^\dagger c_i, \quad (1)$$

where the integrable part of the Hamiltonian representing the kinetic energy term is

$$H_0 = -J \sum_{i=1}^L \left(c_i^\dagger c_{i+1} + c_{i+1}^\dagger c_i \right). \quad (2)$$

In this, c_i^\dagger and c_i are the creation and annihilation operators at i -th site. This system has L lattice sites with periodic boundary conditions applied to it. The onsite potential is $V_i \equiv \cos(2\pi\alpha i)$ and α is a real parameter that modulates the aperiodicity of the lattice. The temporal dependence in the form of Dirac delta function in Eq. 1 ensures that the onsite potential kicks-in whenever $T_n = n\tau$, where n is an integer and τ is the kicking period. The parameter V represents the amplitude of periodic kicks and J is the amplitude for the strength of nearest-neighbour hopping.

Without the train of δ -kicks and if α is an irrational number, then Eq. 1 is the well-known Aubry-André model [34] for electron transport in a lattice with structural disorder. Extensive investigation of this model [35] has shown that if α is a strongly incommensurable number such as the Golden ratio, then all the eigenstates display a transition from extended to localized states at the critical point $V/J = 2$. The transition to localized states has been experimentally observed in the test-bed of non-interacting ultracold atoms in quasiperiodic optical lattices [36], as well as in the interacting case [37]. Numerical evidence too points to the existence of a *many-body* localization transition in the interacting Aubry-André model [38]. The corresponding asymptotic dynamics of an initially localized wavepacket with width σ is ballistic, and the wavepacket width grows as $\sigma_t^2 \sim t^2$, for $V/J < 2$. However, if $V/J > 2$ the spread of the wavepacket is completely suppressed [39], $\sigma_t^2 \sim t^0$. This transition is accompanied by multifractality in the wavefunction [39], diffusive dynamics [40] and a fractal spectrum at the transition point [41, 42]. The dynamics can even be strongly hyperballistic when a quasiperiodic section is embedded in a tight-binding lattice [43].

If the periodic kicks are applied at times $T_n = n\tau$, ($n \in \mathbb{Z}^+$), the critical point for localization transition in

Type of Noise		Description
A	Timing noise (Aperiodicity) [33]	The position of kick (in time axis) is a uniformly distributed random number drawn from the interval $[T - \delta T, T + \delta T]$.
B	Amplitude noise [26]	Kicks are delivered periodically, but after time intervals randomly chosen from Yule-Simon distribution, the amplitude V is altered by a random amount δV .
C	Timing noise (Missed kicks) [27]	The spacing between kicks is a random number drawn from uniform, normal and Poisson distributions and hence some kicks are missed.

TABLE I. Descriptions of three noisy kicking protocols, labeled A, B and C, used in this work. See Fig. 1 for a visual schematic of these protocols.

the limit of high-frequency of kicks is found to be $\frac{V}{JT} \sim 2$ [44]. However, if this critical point is approached from the delocalized phase, the system exhibits a range of growth rates; *i.e.*, $\sigma_t^2 \sim t^\gamma$, $1 \leq \gamma \leq 2$, with a sharp fall-off to $\sigma_t^2 \sim t^0$ for $V > 2JT$ [33].

B. Classical limit

In the classical limit, the Hamiltonian in Eq. 1 exhibits chaotic dynamics since kicking eliminates energy as a conserved quantity. This can be seen in the classical Hamiltonian obtained by taking a continuum limit of the kicked tight-binding model as follows :

$$\begin{aligned} \sum_x |x\rangle\langle x+1| &\rightarrow \exp(-i\hat{p}) \\ \sum_x |x+1\rangle\langle x| &\rightarrow \exp(i\hat{p}). \end{aligned} \quad (3)$$

$$\begin{aligned} -J \sum_{i=1}^L (c_i^\dagger c_{i+1} + c_{i+1}^\dagger c_i) &= -J \sum_x (|x\rangle\langle x+1| + |x+1\rangle\langle x|), \\ &= -2J \cos(\hat{p}) \end{aligned} \quad (4)$$

$$H_{cl} = -2J \cos(p) + V \sum_n \delta(t - T_n) \cos(2\pi\alpha x). \quad (5)$$

Starting from H_{cl} we can derive the so-called kicked Harper map [45],

$$\begin{aligned} p_{n+1} &= p_n + 2\pi\alpha V \sin(2\pi\alpha x_n), \\ x_{n+1} &= x_n + 2J\tau \sin(p_{n+1}). \end{aligned} \quad (6)$$

Numerical investigations have shown that such a model is chaotic regardless of the value of α , leading one to posit that all kicked tight-binding models ought to be quantum chaotic. Numerous studies on this map [45–47] have effectively established what is known about the Aubry-André-Harper model to be true even in the presence of kicking, with the addition of intriguing dynamics such as

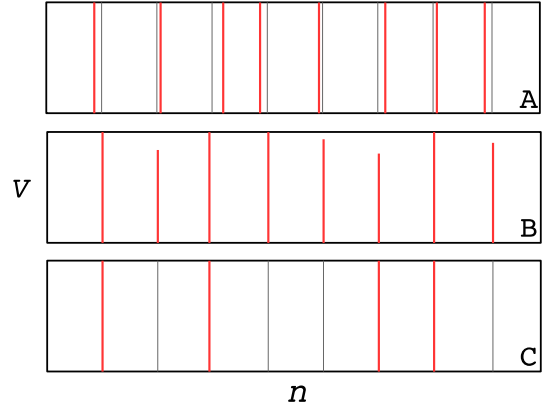


FIG. 1. Schematic of noisy kicking protocols. Kick amplitudes are shown as a function of integer time n . Grey color vertical lines are the positions of kicks had the kick sequence been periodic. Red colour lines indicate the actual kicks imparted for the given type of noise protocol. Labels A, B and C refer to three kicking protocols (see Table I).

ballistic transport *and* quantum localization, depending on the location in (semi-classical) phase space [45]. These have been corroborated by studies on their tight-binding analogues which have begun to be explored only recently [33, 44].

III. NOISY DRIVING : PROTOCOLS AND METHODS

In this section, results related to the dynamical effects that arise from a stochastic perturbation to the driving term in Hamiltonian in Eq. 1 are presented. Indeed, some effects of aperiodicity in the kicking have been studied previously [33], where it was found that localization persists even in the presence of strong aperiodicity for sufficiently long time. The kicking protocol used was such that the time interval between kicks was drawn uniformly from an interval $(T - \delta T, T + \delta T)$. Against this backdrop, in this paper, the AAH model has been subject to stronger forms of noise protocols in order to probe the range of phenomena that driving, periodic or noisy, can elicit. In this paper, noise protocols were implemented by modifying the periodic potential in Eq. 1 to

$$\sum_n (V + \delta V_n) g_n \delta(t - n\tau) \sum_{i=1}^L V_i c_i^\dagger c_i. \quad (7)$$

These noisy protocols are listed in Table I. The case of the periodic kick sequence corresponds to $g_n = 1$ and $\delta V_n = 0$ for all n . Protocol A, shown in Fig. 1(A), corresponds to $g_n = 1$ and $\delta V_n > 0$ for all n , and its outcome has been reported before [33]. In this protocol, white noise is superimposed on kick times [33] such that, on an average, there is still one kick during every time period τ though the actual positions of kicks are noisy.

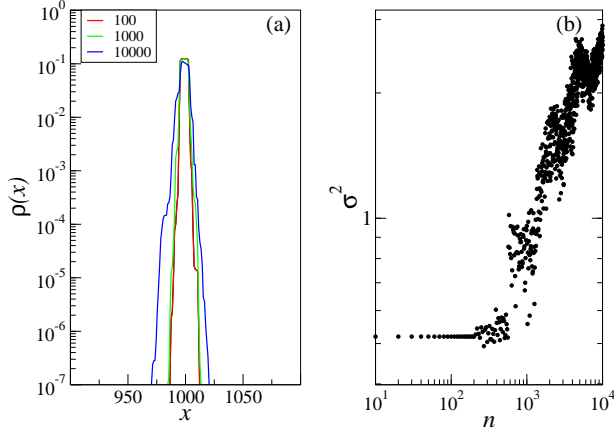


FIG. 2. Density profile $\rho(x)$ and spread of the wavefunction under protocol B. (a) $\rho(x)$ at times $n = 100, 1000$ and 10000 . (b) Width of the time evolving wavefunction (indicated by σ^2). In this, timing noise is drawn from a Yule-Simon distribution with exponent $\beta = 0.75$ and amplitude noise is uniformly distributed in the range $[-V/2, V/2]$.

In protocol B, visualized in Fig. 1(B), a kick is always delivered at periods of τ and hence $g_n = 1$. However, after time intervals drawn from Yule-Simon distribution given by

$$f(k) = \beta B(k, \beta + 1) \xrightarrow{k \rightarrow \infty} k^{-\beta-1},$$

the amplitude is made noisy ($\delta V_n > 0$) and is drawn from a uniform distribution. In this, B is the Beta function and β is a parameter. In protocol C, $\delta V_n = 0$ and g_n takes either 0 or 1. If $g_n = 0$ ($g_n = 1$), kicks are missed (present). The time interval between successive occurrences of 1 is $K_n \tau$ with K_n being an integer drawn from uniform, Poisson or normal distributions.

In this work, the evolution of a wavepacket, initially localized at the center of the lattice, is characterized by two quantities – its (noise-averaged) spread $\sigma^2(t)$ and an instantaneous, locally averaged diffusion exponent γ_m , defined as follows :

$$\sigma^2(t) = \sum_{i=1}^N (i - N/2)^2 \overline{|C_i(t)|^2}; \quad C_i(t) \equiv \langle x_i | \psi(t) \rangle, \quad (8)$$

$$\gamma_m(t) \equiv \frac{1}{m} \sum_{\bar{t}=-\frac{m}{2}}^{\frac{m}{2}} \frac{\log(\sigma^2(t + \bar{t})) - \log(\sigma^2(t))}{\log\left(1 + \frac{\bar{t}}{t}\right)}. \quad (9)$$

The utility of γ_m lies in its ability to expose local variations in the dynamics. The caveat, then, is that genuine local fluctuations need to be aptly distinguished from noise, especially in the cases where the system is aperiodically driven.

The numerical results shown in this paper were implemented using the Armadillo linear algebra library [48, 49]. The initial wavefunction, placed at the middle of the lattice of size L , $\langle x | \psi(t=0) \rangle = \delta_{x, L/2}$ is evolved under the action of noisy kicks applied to the Hamiltonian

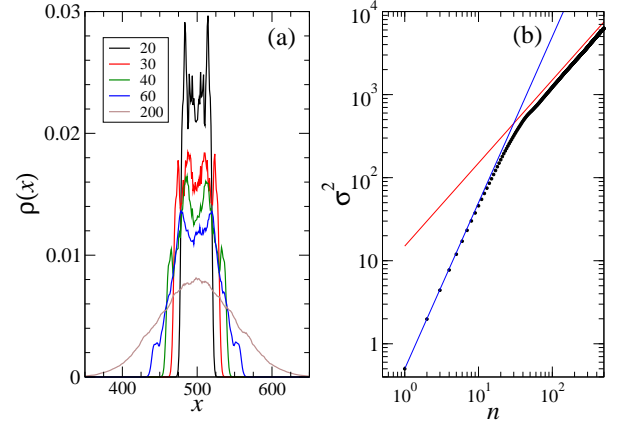


FIG. 3. Density profile $\rho(x)$ and its evolution under protocol C for parameters $V = 1.5$ and $A = 50$. (a) $\rho(x)$ at times $n = 20, 30, 40, 60$ and 200 . (b) Width of the time evolving wavefunction as a function of time. The dashed lines have slopes 1 and 2. See text for details of noise imposed on kick sequence.

in Eq. 1. If the kicks are periodically applied (noiseless case), then the wavefunction at every time step is acted upon by the unitary operator

$$U(\tau^-, 0^-) = e^{-i\tau \hat{H}_0} e^{-i\hat{V} \Delta t}, \quad (10)$$

with $\Delta t = \tau$ only for the strictly periodic case. The superscript ‘-’ indicates the mapping of the system between two instants immediately before kicks. In noisy cases, the operator $e^{-i\tau \hat{H}_0}$ is applied at every time step while the kicking potential e^{-iV} , $\hat{V} = V \sum_{j=1}^L \cos(2\pi \alpha j + \phi) c_j^\dagger c_j$ is applied at times t_n and the time interval Δt will be a random variable as per the protocols listed in Table I. Apart from these noisy protocols, the case where the kick operator $e^{-i\tau \hat{V}}$ is applied based on the result of a biased coin-toss provides an insight into the role played by the correlations in the kicks. This is discussed in section VII(D). All these are implemented by direct matrix multiplication, since \hat{H}_0 is tridiagonal in the position basis, and can be efficiently diagonalised and hence exponentiated.

IV. EVOLUTION UNDER NOISY KICKS

A. Noisy kicks versus missing kicks

For the purposes of the numerical results presented in this section, the parameters for the noise-free AAH model are set at $\tau = 0.5$ and $J = 1$ resulting in $V_c \sim 2J\tau = 1$ at which the delocalization to localization transition takes place. To motivate the main results, two broad scenarios arising from the application of protocols B and C are displayed in Fig. 2 and 3. The density profile of the evolving wavepacket and $\sigma^2(n)$ are shown in Fig.

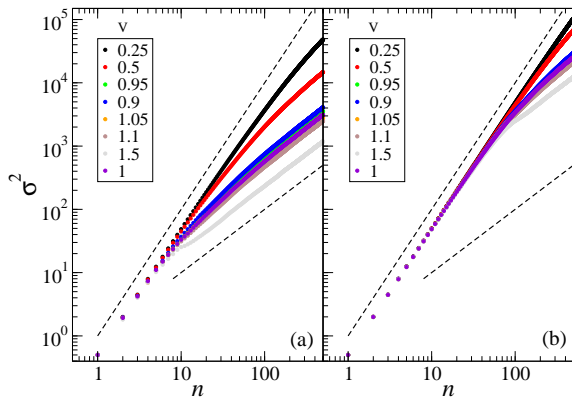


FIG. 4. Wavefunction evolution under the effect of missed kicks (protocol C), with the time intervals without kicks are drawn from uniform distribution. Width of the evolving state σ vs. time (symbols) shown for several values of kick strength V with (a) $A = 10$ and (b) $A = 100$. For $V > V_c$, a sharp break in the dynamics is observed at $n = n_c \sim A$. The dashed lines have slopes 1 and 2.

2(a,b) for protocol B. Remarkably, when the model is in the localized phase ($V = 1.5$), despite strong amplitude noise with a width equal to V , the density profile nearly retains its shape. The corresponding growth of $\sigma^2(n)$ is so strongly muted that it is of $O(1)$ even after 10^4 time steps. A similar scenario of robust localization emerges if protocol A is applied (not shown here) and this has been reported before in Ref. [33].

Hence, in any protocol that ensures that a kick is consistently delivered at multiples of τ , or at least in a small time window around it [33], the wavepacket spread is weakly subdiffusive, indicating the robustness of the localized phase to noise. Even if the amplitude is altered at a random time, localization persists for an extensive number of kicks, as evident in Fig. 2(a,b). This picture changes when a kick is not guaranteed at every timestep as in the case of protocol C displayed in Fig. 1(c). If T_N is the time at which the N -th kick is delivered, then $K_N \equiv (T_{N+1} - T_N)/\tau$, where $K_N > 0$ is an integer random variable drawn from a discrete distribution $F(K)$. In the rest of the paper, we shall call $F(K)$ the waiting time distribution since it represents the time interval between successive appearance of kicks.

As we show in the next section, the character of diffusion undergoes a sharp change at a timescale decided by the specifics of the noise process. This is observed across different types of noise superimposed on the standard kick sequence. Figure 3(a) shows the evolution of density profile due to noisy protocol C. A global picture is seen in Fig. 3(b). At short timescales, the dynamics can display **subdiffusive** to ballistic growths, and tends asymptotically towards diffusive dynamics. This crossover from growth with slope 2 (in log-log plot) to slope 1 is observed in Fig. 3(b). If n_c represents this crossover timescale, then superdiffusive growth takes place for times $n < n_c$, and becomes diffusive for $n > n_c$. The numerical value

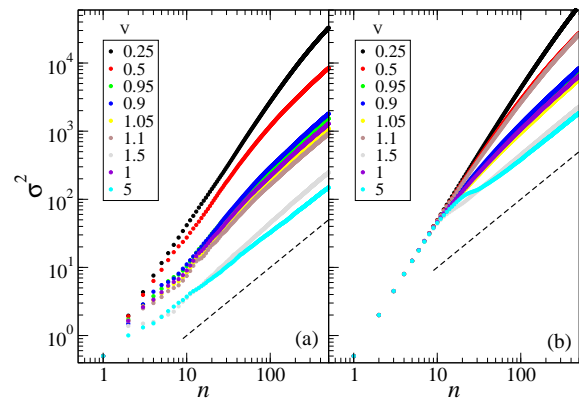


FIG. 5. Wavefunction evolution under the effect of missed kicks (protocol C), with waiting times drawn from Poisson distribution. Width of the evolving state σ vs. time (symbols) shown for several values of V for (a) $\lambda = 0.5$ and (b) $\lambda = 10$. Note the sharp transition point for $\lambda = 10$. Dashed lines have slopes 1 and 2.

of n_c is dependent on the properties of superimposed noise. Given that localization is robust even if noisy kicks are imparted once every kicking period, in the subsequent sections, we focus on the wavefunction evolution under the effect missed kicks (protocol C). In the limit of $t \rightarrow \infty$, the unbounded diffusive growth continues though in practice it is interrupted by the finite size of the lattice.

V. DYNAMICS UNDER MISSING KICKS

In this section, the diffusive effects induced by the missing kicks, protocol C, are studied. To begin with, since $K \in \mathbb{Z}$, we consider the case of $F(K)$ being a discrete uniform distribution $U(K; A)$, with $K \in [1, A]$ defining the support for the distribution. In this case, a ballistic growth at initial times and an asymptotic diffusive growth is generically observed. The simulations that result from the Hamiltonian in Eq. 1, shown in Fig. 4, reveal the existence of a crossover timescale n_c . In Fig. 4(a), σ^2 is shown as a function of n for several values of kick strength V for $A = 10$. At short time scales of $n < n_c$, the wavefunction spread is ballistic as the increase in σ^2 is parallel to dashed line with slope 2. For $n > n_c$, wavefunction spread becomes diffusive, as evident in $\sigma^2(n)$ becoming parallel to a line with slope 1 (Fig. 4(a)). This scenario of transition from ballistic growth at short times to asymptotic diffusive growth repeats for $A = 100$ as well, as shown in Fig. 4(b).

When the kicking is in the delocalized regime, $V < V_c$, then the transition is smooth and is corroborated in Fig. 4(a). However, in the cases when $V \gtrsim V_c$, the transition suddenly sharpens, and one can notice distinct regimes in the dynamics. In this case, a distinct crossover point between the two regimes is observed. A common feature is that regardless of the number of distinct regimes, transitions between them are always sharp and hence we can

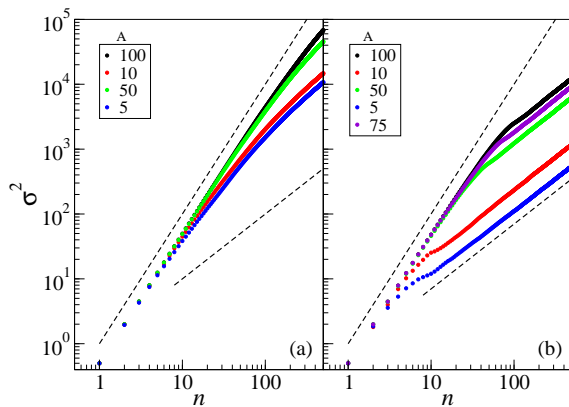


FIG. 6. Growth of density profile in the delocalized and localized regime as the parameter A of the waiting time distribution $U(K; A)$ varies. In this, (a) $V = 0.5$ and, (b) $V = 1.5$ are fixed, but A is varied. Abrupt transitions from superdiffusive to diffusive growth is seen only in the localized regime with $V > V_c$. Dashed lines have slopes 1 and 2.

label them as being distinct. In particular, for $V > V_c$, the transition to asymptotic diffusive behaviour always occurs at $n = n_c \approx A$. This is borne out by the numerical results in Fig. 4(a,b). The asymptotic diffusive behaviour is expected as a generic feature of decoherence [50], which takes place when noise is introduced into a system [24, 51].

If the waiting times are Poisson distributed, *i.e.*, $F(K) = P(K; \lambda)$, where λ is the mean of the distribution, a scenario similar to that of uniform distribution emerges. For $\lambda < 1$, which physically implies that kicks are rarely missed, the dynamics of the almost periodically kicked Hamiltonian gives rise to approximately ballistic initial growth until asymptotic diffusive growth sets in at later times. The timescale at which this sets in is much longer when $V < 1$ than if $V > 1$. These features are observed in the simulation results in Fig. 5(a) for which $\lambda = 0.5$. In all the cases, asymptotic diffusive growth sets in as $n \gg 1$. For large λ , as shown in Fig. 5(b), there is an initial ballistic growth and it crosses over to normal diffusion, as in the case of uniform noise. The transition point n_c from superdiffusive to diffusive growth is sharp if $V > 1$, and it is smooth if $V < 1$.

What is the nature of transition if the parameter characterising the waiting time distribution is varied? The qualitative picture portrayed in Fig 4 does not change even if the parameter A in the uniform waiting time distribution $U(K; A)$ is varied. As displayed in Fig. 6, varying A does not modify the initial superdiffusive regime and the asymptotic diffusive regime. Its effect is to simply shift the time at which the sharp transition is observed for $V > V_c$ (Fig. 6(a)), and to change the timescale on which asymptotic diffusion sets in for $V < V_c$ (Fig. 6(b)). The distinct dynamical behaviour upon variation of λ is evident in Fig. 7. No sharp transitions are observed for $V < 1$, irrespective of the value of

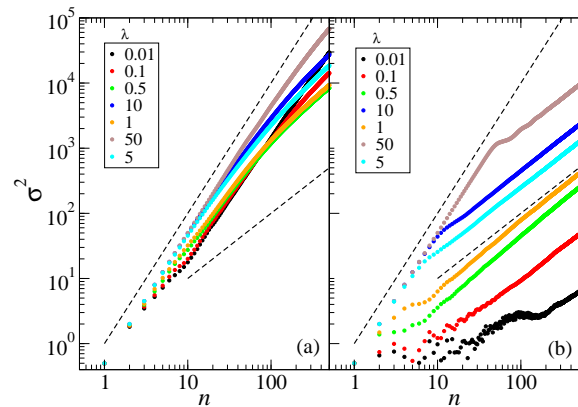


FIG. 7. Growth of density profile in the delocalized and localized regime with the change in the parameter λ of the waiting time distribution $P(K; \lambda)$. In this, (a) $V = 0.5$ and, (b) $V = 1.5$ are fixed, but λ is varied. Sharp transitions from superdiffusive to diffusive growth is seen only in the localized regime with $V > V_c$ and $\lambda \gg 1$. Dashed lines have slopes 1 and 2.

λ . In this case, all the transitions are smooth as seen in Fig. 7(a). For large λ , longer mean waiting times ensure that the ballistic regime stays on for longer timescales. On the other hand, for $V > 1$ sharp ballistic to diffusive transitions are observed if $\lambda > 1$ (Fig. 7(b)). In section VII, we provide a justification for these observations and also for the qualitative similarity of the dynamics with Poisson noise ($\lambda \gtrsim 2$) to that of uniform noise. Thus, the parameters A and λ effectively tune the separation of timescales with distinct growth regimes. Further, similar results as in Figs. 4-7 were also observed (not shown here) when K_n were chosen as the integer parts of a normally distributed variable.

VI. TRANSLATIONALLY INVARIANT MODELS

In the light of the results presented above, one significant question of interest would be the dependence of the observed phenomena on the lack of translational invariance in the model. To address this, the parameter α in the onsite potential V_i in Eq. 1 is tuned from rational to an irrational number. A standard way to do this is to consider a sequence α_i such that $\alpha_i = F_i/F_{i+1}$, where F_i is the i^{th} Fibonacci number. Then, $\lim_{i \rightarrow \infty} \alpha_i = \frac{\sqrt{5}-1}{2}$. When $\alpha = \frac{p}{q}$, where p and q are integers, the Hamiltonian in Eq. 1 becomes translationally invariant and will have q -bands under periodic driving. In this section, we simulate the wavefunction evolution for the q -band model and obtain σ^2 as a function of time n .

Firstly, as Figs. 8 and 9 show, a transition from ballistic to diffusive growth of σ persists even in the translationally invariant models. Further, the transition is sharp under identical parametric regimes, *i.e.*, $V > V_c$,

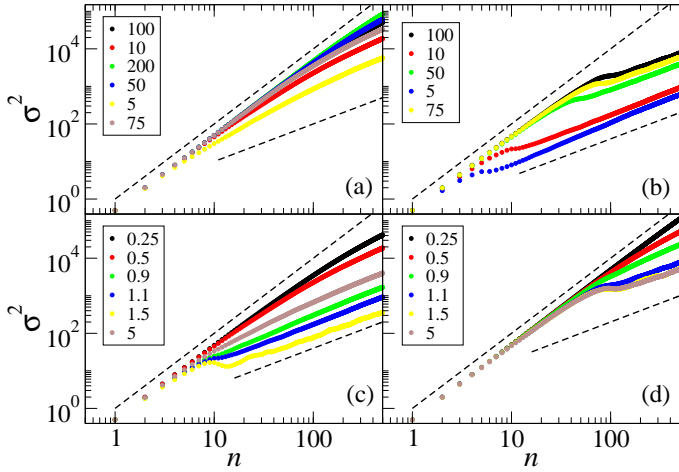


FIG. 8. Diffusion in 2-band model with uniformly distributed waiting times between kicks. The parameters are (a) $V = 0.5$ and (b) $V = 1.1$ for various values of A , and (c) $A = 10$ and (d) $A = 100$, for various values of kicking strength V . Dashed lines have slopes 1 and 2.

considered earlier in Figs. 6 and 7. As the system is switched from a free model to a q -band model, where q is a small integer, it is surprising to observe a sharp break connecting these two regimes. In the simulations with 2-band model and noisy protocol C with uniform waiting time distributions, sharp transition is absent if $V < V_c$ whereas it is clearly visible if $V > V_c$ as seen in Figs. 8(a,b,c,d). In the case of Poisson distributed waiting times shown in Fig. 9 a sharp transition is seen if $\lambda \gg 1$. The asymptotic diffusive dynamics in all the cases arises due to decoherence. Such dynamics is generically seen across all the q -band structures we have simulated for $2 \leq q \leq 10$. Hence, the results shown in Figs. 4 to 7 are also valid for models with translational invariance.

In general, what determines if the nature of transition will be sharp or smooth? Further, in certain windows of the strength of kicks V , a drastic slowing down in the growth of σ at the transition point is observed. This is accompanied by the diffusion exponent almost reaching zero and, in certain cases, even falling further. To explain the observed features in Figs. 4 to 9, we further study the band structure of the 2-band model in greater detail.

A. Band Structures : kicking induced flat bands

A first striking observation from the band structures is that, for the model in Eq. 2, kicking alone can be used to engineer flat-bands and hence, the localization of excitations. Lattice models that exhibit flat bands have been of considerable interest in recent times [52–54]. An effective Hamiltonian which gives rise to the same dynamics as that of the periodically driven model over one time period can be obtained from the Floquet opera-

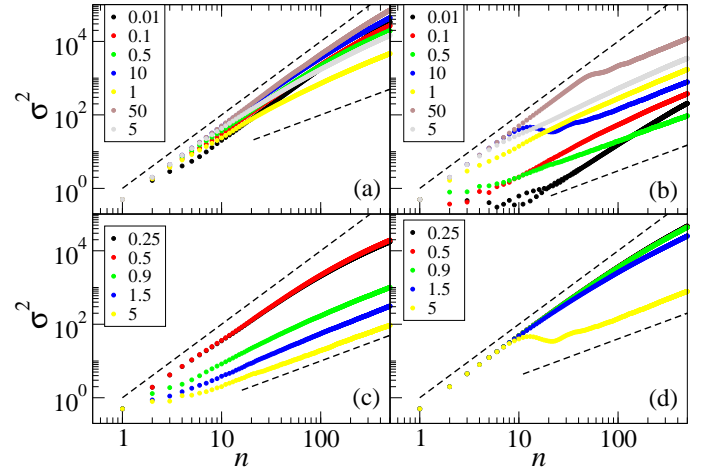


FIG. 9. Diffusion in 2-band model with Poisson distributed waiting times between kicks. The parameters are (a) $V = 0.5$ and (b) $V = 1.1$, for various λ , and (c) $\lambda = 0.5$ and (d) $\lambda = 10$, for various V . Dashed lines have slopes 1 and 2.

tor using the Baker-Campbell-Hausdorff expansion. In a naïve weak-potential approximation at high kick frequencies, one simply obtains an effective Hamiltonian $H_{\text{eff}} = \hat{H}_0 + \hat{V}/\tau$, leading to a tight-binding model with the potential rescaled by τ . However, for no on-site potential of finite strength can there be flat bands in static q -band tight-binding models. Analytically, this can be seen for the simple cases of the 2, 3 and 4 band models. Concretely, the dispersion relation for a 2-band model with onsite potentials $\pm\mathcal{U}$ is given by [55]

$$E(k) = \pm \sqrt{\mathcal{U}^2 + 4J^2 \cos^2\left(\frac{ka}{2}\right)}, \quad (11)$$

where a is the lattice spacing, and J is the hopping amplitude. Only in the limit where the hopping is completely suppressed and there are on-site potential terms alone, is the spectrum flat.

Evidently, this is not the case for the kicked AAH model in Eq. 1. Figure 10 shows the band structure for the 2-band model. As seen in Fig. 10(d), flat bands can indeed be realised with finite on-site potential in the presence of kicking. By diagonalising the Floquet operator, the quasi-energies $\epsilon(k)$ can be expressed as

$$\epsilon(k) = \pm \cos^{-1} \{ \cos(2J\tau \cos k) \cos V \}. \quad (12)$$

Thus, flat-bands exist for $V = (2l+1)\frac{\pi}{2}$, $l \in \mathbb{Z}$ and the kicking has shown a relatively straightforward mechanism to construct flat bands. This is confirmed in Fig. 10(d) where flat bands appear for $V = \pi/2 \approx 1.55$. At such parameter values, where the allowed bands are exactly flat, an abrupt transition point is indeed observed (Fig. 8(c,d)).

However, as simulation results reveal, *perfectly* flat bands are not required in order to observe either a

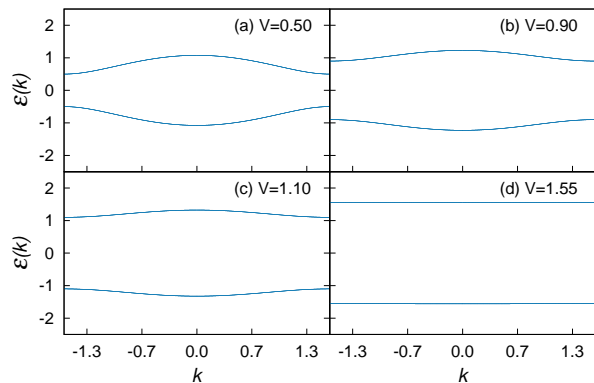


FIG. 10. Band structures obtained from simulations for the 2-band model. Note that the flat bands are obtained for $V = \pi/2 \approx 1.55$.

sharp break or a slowing down in the dynamics. For instance, sharp transitions begin to appear approximately for $V > V_c$ as seen in Fig. 8(c,d). Hence, in the next section, we provide analytical support to the observations in sections III to VI using 2-band model. In particular, we also analyse the question, how “flat” is “flat enough”? Moreover, are there other transitions that one can expect to observe that accompany the appearance of a break in the dynamics?

VII. ANALYSIS

In this section, analytical justification is presented, mainly, for the case 2-band model. Firstly, γ_4 , as defined in Eq. (9), is computed to obtain n_c , the time at which sharp transition takes place in the dynamics. Secondly, as a further evidence for sharp transtion at time $n = n_c$, a naïve scaling of $\log(\sigma^2)$ is presented in the case of uniform noise. Finally, the role of noise correlations in the sharpness of the transition is elucidated.

A. Calculation of γ_4

The time n_c at which the dynamics sharply transitions from superdiffusive to diffusive is obtained by calculating the averaged local diffusion exponent γ_m , and observing the time at which sharpest drop occurs. As is evident from Figs. 6-7, the transition from initially superdiffusive to diffusive growth is smooth in the delocalized regime of kick strength $V < V_c$. This transition becomes sharp as one approaches and crosses into the localized regime. In our investigations, there does not appear to be any qualitatively different behaviour at the critical point $V = V_c$.

In Fig. 11, for the case of AAH model (Fig. 11(a,b)) and 2-band model (Fig. 11(c,d)), $\gamma_4(n)$ is shown for uniformly distributed waiting times $U(K)$ with $K \in [1, A]$. Clearly, a sharp dip in γ_4 occurs exactly at $n = A$ when

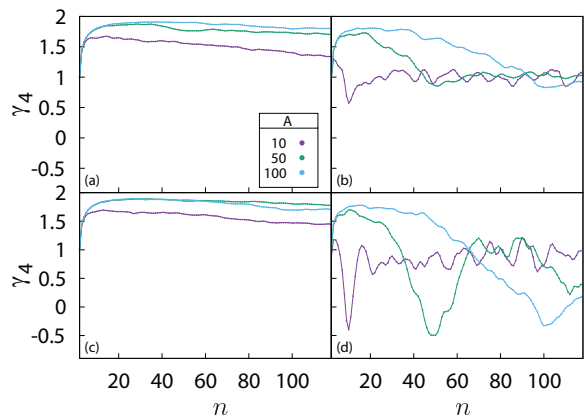


FIG. 11. γ_4 vs. n for noisy models with waiting times drawn from a uniform distribution $U(K)$, with $K \in [1, A]$. (a,b) AAH model, and (c,d) 2-band model. The parameters are (a,c) $V = 0.5$, (b,d) $V = 1.5$.

$V > V_c$. In contrast, for $V < V_c$, a smooth transition occurs from the superdiffusive and diffusive regime.

In fact, the dips in γ_4 in general seem to be far more steep in the translationally invariant case than in the AAH model, across different values of V . As expected, the flatter the bands, the sharper the dips in γ_4 . This provides a quantitative evidence to associate flat bands with sharp transition in diffusive regimes.

B. Scaling of $\sigma^2(t)$

The scaling arguments are presented in this section to corroborate the fact that the time of transition is $n_c \sim A$, when K is drawn from a uniform distribution $[1, A]$.

It can be posited that $\sigma^2(n; A)$ can be expressed in terms of a function σ_0^2 , defined as

$$\sigma_0^2(\bar{n}) = \begin{cases} \bar{n}^2 & 0 < \bar{n} < 1 \\ \bar{n} & \bar{n} > 1 \end{cases}, \quad (13)$$

$$\sigma^2(n; A) = A^2 \sigma_0^2\left(\frac{n}{A}\right). \quad (14)$$

In order to demonstrate this scaling, (the logarithm of) the function $f_A(\bar{n}) \equiv \frac{1}{A^2} \sigma^2(A\bar{n})$ is plotted for different values of A in Fig. 12. It can be seen from this figure that $f_A(\bar{n}) \sim \sigma_0^2(\bar{n})$ for all A . Taken together, for uniformly distributed waiting times, Figs. 10-12 display the central result that at parametric regimes at which flat bands appear, the transition from superdiffusive to diffusive growth of evolving states is sharp, and the transition point follows a excellent scaling with respect to a parameter A that controls the strength of noise.

C. Mechanisms for time of transition and diffusion

In this section, analytical support is provided for associating flat bands with the sharp superdiffusive to diffusive transition in the case of 2-band model. To begin, the following three probabilities are defined:

$\mathcal{P}(n) \equiv$ the probability of a kick occurring at the n^{th} time step

$P_N(n) \equiv$ the probability of the N^{th} kick occurring at the n^{th} time step

$Q(n; N) \equiv$ the probability that exactly N kicks have been received before the n^{th} time step

These quantities are related to each other as

$$\mathcal{P}(n) = \sum_{N=1}^n P_N(n) \quad (15)$$

$$Q(n; N) = \sum_{n'=N}^n (P_N(n') - P_{N+1}(n')). \quad (16)$$

If t_i , $i = 1, 2, \dots, N$, denote the time intervals between successive kicks on the time axis, then the calculation of $P_N(n)$ amounts to finding the number of ways one can choose $\{t_1, t_2, \dots, t_N\}$ such that $\sum_{i=1}^N t_i = n$. Thus

$$P_N(n) = P_N\left(\sum_{i=1}^N t_i = n\right) \quad (17)$$

For the specific case of $F(K) = U(K; A)$, note that $P_N(n) = 0$ if $N < \lceil \frac{n}{A} \rceil + 1$, and by construction, $P_N(n) = 0$ if $N > n$ for all cases of $F(K)$. The normalisation condition is

$$\sum_{n=N}^{NA} P_N(n) = 1 \quad (18)$$

from which one can see that

$$\begin{aligned} Q(n \geq (N+1)A; N) &= \sum_{n'=N}^n (P_N(n') - P_{N+1}(n')) \\ &= \sum_{n'=N}^{NA} P_N(n') - \sum_{n'=N+1}^{(N+1)A} P_{N+1}(n') \\ &= 1 - 1 = 0. \end{aligned} \quad (19)$$

The last form uses the normalization in Eq. 18. In all cases, $\mathcal{P}(n)$ does depend on n , at least for small n .

This discussion begins by considering what happens to an initial state ψ_0 under the dynamics of the 2-band model after the system receives exactly one kick. The quantity of interest, then, is

$$\begin{aligned} \tilde{\sigma}^2(t_1, t_2, V) &\equiv \langle \psi_0 | e^{it_1 \hat{H}_0} e^{i\hat{V}} e^{it_2 \hat{H}_0} \hat{x}^2 e^{-it_2 \hat{H}_0} e^{-i\hat{V}} e^{-it_1 \hat{H}_0} | \psi_0 \rangle; \\ |\psi_0\rangle &\equiv \frac{1}{\sqrt{L}} \sum_k |k\rangle. \end{aligned} \quad (20)$$

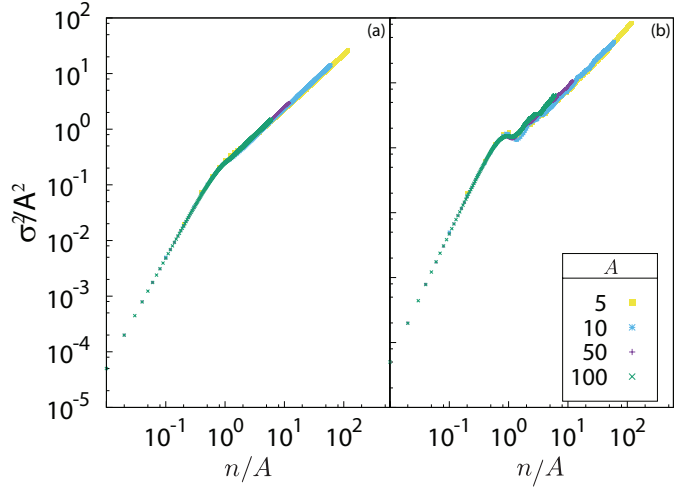


FIG. 12. Scaling of σ^2 with the A for the case of uniformly distributed waiting times with $V = 1.5$. (a) AAH model, and (b) 2-band model. Note the excellent data collapse after scaling using Eq. 14.

where $|k\rangle$ are the momentum states. In the momentum basis, the evolution operator decomposes into 2×2 subspaces, in which, \hat{H}_0 is diagonal and $x^2 \rightarrow \sum_{k_1, k_2} \partial_{k_1} \partial_{k_2} \delta(k_1 - k_2)$. The Floquet matrix in a single 2×2 k -subspace is

$$F_k(V, T) = \begin{pmatrix} e^{i2JT \cos k} \cos V & -ie^{i2JT \cos k} \sin V \\ -ie^{-i2JT \cos k} \sin V & e^{-i2JT \cos k} \cos V \end{pmatrix}. \quad (21)$$

After some calculations whose details are given in Appendix A, we obtain

$$\tilde{\sigma}^2(t_1, t_2, V) = 2(J\tau)^2 (t_1^2 + t_2^2 + 2\cos(2V)t_1 t_2). \quad (22)$$

For perfectly flat bands $V = \frac{\pi}{2}$, and this reduces to

$$\tilde{\sigma}^2(t_1, t_2, \pi/2) = 2(J\tau)^2 (t_1 - t_2)^2. \quad (23)$$

This can be interpreted as follows. An impulse with a flat band Hamiltonian leads to a reversal of the velocity of the wavepacket. Concretely, consider the case where $F(K) = U(K; A)$. The probability that the system has received only one kick by the time $n = A$ steps have elapsed is

$$Q(A; 1) = \left(\frac{1}{2} + \frac{1}{2A}\right) > \frac{1}{2}. \quad (24)$$

Under the assumption that the system is faced with this, the most probable scenario for σ would be

$$\sigma^2(A\tau) \sim \frac{(J\tau)^2}{3} A(A+2) \sim \frac{1}{6} \tilde{\sigma}^2(A, 0, 0). \quad (25)$$

The leading order term here shows that while the coefficient has reduced, the dynamics is still ballistic. However, when one considers time steps $n > A$, it is most

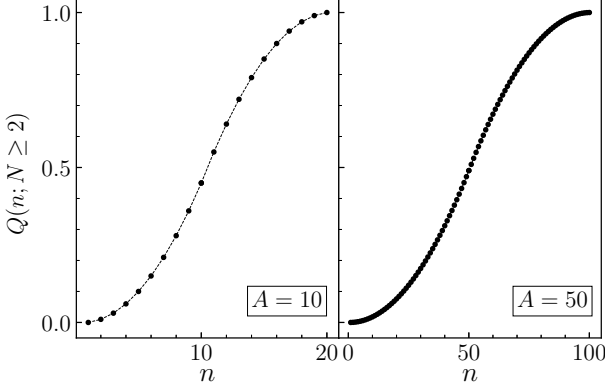


FIG. 13. Cumulative mass function $Q(n; N \geq 2)$ for $F(K) = U(K; A)$. The transition happens at time n_c such that $Q(n; N \geq 2) = \frac{1}{2}$. This figure shows that $n_c \sim A$.

likely that the system will have seen at least 2 kicks (details of the calculation in Appendix B) and its probability can be expressed as

$$Q(n > A; N \geq 2) = 1 - Q(n > A; 1) - Q(n > A; 0) > \frac{1}{2}. \quad (26)$$

As more kicks are imparted, the particle is subject to an increasing number of velocity reversals, and it executes a random walk, leading to diffusive behaviour.

Based on this argument, we posit that the break-time n_c is the time at which $Q(n; N \geq 2)$ – a monotonic, increasing function – exceeds $\frac{1}{2}$. Then, for $n > n_c$, the system has most likely received more than one kick. The quantity of interest $Q(n; N \geq 2)$ is shown to be the Cumulative Mass Function (CMF) for the distribution $P_2(n)$ in Appendix B. Thus, the posited break-time is the median of the distribution $P_2(n)$ which is A , for the case of uniform noise and $\sim \lambda$ for $\lambda \gg 1$, in the Poisson case.

The CMF for the case of uniformly distributed waiting times is shown in Fig. 13, for two different values of A . Using its expression (obtained in Eq. B7 in Appendix B), we obtain $n_c = A$, the value at which CMF becomes larger than $\frac{1}{2}$. This estimate for n_c agrees with the time at which sharp transition is observed in Fig. 6(b).

Similarly, for the case of Poisson waiting time distribution, the CMF is shown in Fig. 14 for various values of mean waiting time λ . In this case, the median of $P_2(n)$ approximately corresponds to the time at which transition to diffusive dynamics takes place. This can be clearly seen for the cases of $\lambda = 5, 10$ upon comparing the median with the actual transition observed in Fig. 7(b). Further, the median occurs at $n > 1$ only when $\lambda \gtrsim 0.7$, and at $n \geq 3$ only when $\lambda \gtrsim 1.25$, which explains why the break is not observable in Fig. 7(b) for $\lambda \leq 1$.

At large times $n \gg 1$, regardless of the form of the $F(K)$, the contribution to $\mathcal{P}(n)$ comes from $P_N(n)$ where

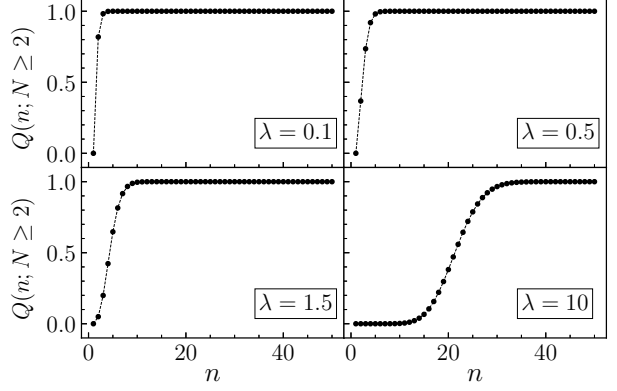


FIG. 14. Cumulative mass function $Q(n; N \geq 2)$ for $F(K) = P(K; \lambda)$. Notice that n_c is barely greater than 1 for $\lambda \leq 1$, explaining why the break is quite abrupt for $\lambda > 1.5$

N is large. By the central limit theorem and Eq. 17, $P_N(n)$ tends to a normal distribution that depends only on the properties of $F(K)$, and thus, $P(n)$ is no longer dependent on n . This implies that the velocity of the particle is reversed with a fixed probability $P_\infty = P(n \rightarrow \infty)$ at each time step. Since the wavepacket evolves with that velocity for one time step, this is akin to a 1-dimensional classical discrete-time random walk. In this case, it is known that $\langle x^2(t) \rangle \sim t$, and hence a linear increase in the square of the width of the wavepacket for $n \gg 1$ can be expected.

D. Role of n dependence of $\mathcal{P}(n)$

From the arguments made in the previous sub-section, it is seems that the time dependence of $\mathcal{P}(n)$ at short times plays a crucial role in the appearance of a sharp transition time n_c . In order to test this, the AAH model in Eq. 1 is evolved and kicks are applied depending on the outcome of a biased coin toss, with various (time-independent) biases. $\mathcal{P}(n)$ is now constrained to be independent of n , as a result, and is denoted by p_k . In the 2-band case, the quantity σ^2 has an exact solution in terms of a 4×4 “disorder matrix”, as shown in Appendix C. The final result turns out to be

$$\sigma^2(N) = \frac{1}{L} \sum_{i,j} [A(N) + B(N) + C(N)]_{i,j}. \quad (27)$$

where $A(N), B(N)$ and $C(N)$ are defined in the Appendix C. Note that the indices in brackets are not the true indices of the 4×4 matrix D . The recipe to switch between the two type of indices is by employing the Kronecker product and is given in Appendix C. The numerically simulated results for the coin-toss model applied to the Hamiltonian in Eq. 1 and for the 2-band model are, respectively, in Fig 15(a) and 15(b). Notice

the absence of sharp transitions even for $V = 1.57$ (at which sharp transitions were observed in the case of uniform and Poisson distributed waiting times). This illustrates another facet of wavefunction spreading – the smooth nature of the crossover from the superdiffusive to the diffusive regime, even at a value of V that produces sharp break-points for other kick sequences with time-dependent $\mathcal{P}(n)$ seems to suggest that this time dependence is crucial to the sharp change observed in the dynamics. This time dependence manifests in form of correlation for the times at which kicks are imparted, in that $\mathcal{P}(n|n') \neq \mathcal{P}(n)\mathcal{P}(n')$. Indeed, there has been work on continuously and stochastically perturbed models where the has played a non-trivial role in engineering such a transition [56].

VIII. CONCLUSIONS

This work had focussed on how an initially localized wavepacket evolves under the action of noisy kick sequences applied to a lattice model with quasi-periodic onsite potential, namely, the Aubry-André model. This system is well known to display localization to delocalization transition even in the one-dimensional case, in contrast to the Anderson model. Periodically driving such systems is known to either preserve localization or induce delocalization depending on the choice of parameters. This work presents an extensive study of effects due to noisy kicks and we place it in the context of the current interest in a variety of Floquet engineering schemes in quantum systems.

In summary, three distinct noisy kick sequences are considered as shown in Fig. 1. The first two sequences deliver one kick on an average in every period, in which case the localized phase appears to be sufficiently robust to application of noise. However, if the kick sequence is

chosen such as to miss certain kicks entirely, then the results are quite dramatic. Most of this paper discusses the effects due to randomly missed kicks. Under these conditions, it is found that the dynamics of an initially localized wavepacket can be made ballistic for arbitrarily long times by tuning a parameter characterising the noise process. Following the ballistic regime, there is a sharp transition to diffusive behaviour. In particular, the transition is not always smooth. This was observed both in translationally invariant as well as disordered models; the former required some degree of flatness to the bands. We argue and show, using a 2-band model, that the emergence of diffusive behaviour in the long time limit is intrinsically linked to velocity reversals which leads to classical random walk type behaviour. More importantly, by using an uncorrelated kick sequence for comparison, it is shown that correlations in the noise play a crucial role in facilitating the sharpness of this transition, which is determined by the parameters characterising the noise realizations.

It would be interesting to obtain a more rigorous analytic backing for the criterion to find the ballistic to diffusive transition timescale n_c . Moreover, the observation of these phenomena in the presence of interactions is yet to be explored in this model, but results in continuously (stochastically) driven models that could serve as guides to future studies [56].

ACKNOWLEDGMENTS

We are grateful to G. J. Sreejith for helpful discussions and comments on the thesis that led to this work. One of the authors (MSS) would like to acknowledge the financial support from Science and Engineering Research Board, Govt. of India, through MATRICS grant MTR/2019/001111.

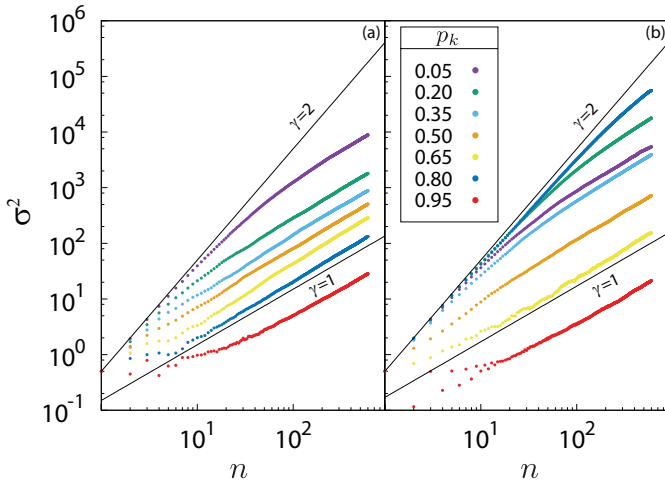


FIG. 15. σ^2 vs. t/τ at $V = 1.57$ for coin-toss noise in the (a) AAH model and (b) 2-band model

Appendix A: Calculation of $\tilde{\sigma}^2(t_1, t_2, V)$

Let $U_{k1} \equiv F_k(V, t_2)F_k(0, t_1)$, where $F_k(V, T)$ is the same as in Eq. (21). $\tilde{\sigma}^2(t_1, t_2, V)$, as defined in Eq. (20), can equivalently be written as

$$\begin{aligned}
 & \frac{1}{L} \sum_{\substack{\{i_n, j_n\} \\ k_1, k_2}} \langle i_0 | U_{k_2}^\dagger | i_1 \rangle \langle j_1 | U_{k_1} | j_0 \rangle \frac{\partial^2 \delta(k_1 - k_2)}{\partial k_1 \partial k_2} \\
 &= \frac{1}{L} \sum_{\substack{\{i_n, j_n\} \\ k_1, k_2}} \frac{\partial}{\partial k_2} \langle i_0 | U_{k_2}^\dagger | i_1 \rangle \frac{\partial}{\partial k_1} \langle j_1 | U_{k_1} | j_0 \rangle \delta(k_1 - k_2) \delta_{i_1, j_1}
 \end{aligned} \tag{A1}$$

$\{i_n, j_n\} = 1, 2$ and $k_1, k_2 \in [0, \pi)$.

$$\begin{aligned} \frac{\partial}{\partial k_1} \sum_{j_0} \langle j_1 | U_{k_1} | j_0 \rangle = (-\iota 2J \sin(k_1)) \times \left\{ \right. \\ \delta_{j_1,1} \left((t_1 + t_2) \cos(V) e^{\iota 2J(t_1+t_2) \cos(k_1)} + \right. \\ \left. \iota(t_1 - t_2) \sin(V) e^{-\iota 2J(t_1-t_2) \cos(k_1)} \right) - \\ \delta_{j_1,2} \left(-(t_1 + t_2) \cos(V) e^{-\iota 2J(t_1+t_2) \cos(k_1)} + \right. \\ \left. \iota(t_1 - t_2) \sin(V) e^{\iota 2J(t_1-t_2) \cos(k_1)} \right) \left. \right\} \quad (\text{A2}) \end{aligned}$$

$$\begin{aligned} \frac{\partial}{\partial k_2} \sum_{i_0} \langle i_0 | U_{k_2}^\dagger | i_1 \rangle = (-\iota 2J \sin(k_2)) \times \left\{ \right. \\ \delta_{i_1,1} \left(-(t_1 + t_2) \cos(V) e^{-\iota 2J(t_1+t_2) \cos(k_2)} + \right. \\ \left. \iota(t_1 - t_2) \sin(V) e^{\iota 2J(t_1-t_2) \cos(k_2)} \right) + \\ \delta_{i_1,2} \left((t_1 + t_2) \cos(V) e^{\iota 2J(t_1+t_2) \cos(k_2)} - \right. \\ \left. \iota(t_1 - t_2) \sin(V) e^{-\iota 2J(t_1-t_2) \cos(k_2)} \right) \left. \right\} \quad (\text{A3}) \end{aligned}$$

Using these results, redefining $t_i \rightarrow t_i/\tau$ and some straightforward calculations, one arrives at

$$\begin{aligned} \tilde{\sigma}^2(t_1, t_2, V) = \frac{8}{L} \left(\sum_k \sin^2(k) \right) \times \\ (J\tau)^2 \left((t_1 + t_2)^2 - 4 \sin^2(V) t_1 t_2 \right). \quad (\text{A4}) \end{aligned}$$

Replacing $\frac{1}{L} \sum_k \sin^2(k) \rightarrow \frac{1}{2\pi} \int_0^\pi dk \sin^2(k) = \frac{1}{4}$, we have

$$\tilde{\sigma}^2(t_1, t_2, V) = 2 (J\tau)^2 (t_1^2 + t_2^2 + 2 \cos(2V) t_1 t_2) \quad (\text{A5})$$

Appendix B: Calculation of $Q(n; N \geq 2)$

1. General form of $Q(n; N \geq 2)$

We begin by considering $Q(n; N = 0)$, which is the probability that no kick has been imparted to the system until step n . From the definition,

$$Q(n; 0) = \sum_{n'=n+1}^n P_1(n') \quad (\text{B1})$$

$$= 1 - \sum_{n'=1}^n P_1(n') \quad (\text{B2})$$

$$\begin{aligned} Q(n; 1) &= \sum_{n'=1}^n (P_1(n') - P_2(n')) \\ &= 1 - Q(n; 0) - \sum_{n'=1}^n P_2(n') \end{aligned}$$

$$\sum_{n'=1}^n P_2(n') = 1 - Q(n; 1) - Q(n; 0)$$

$$Q(n; N \geq 2) = \sum_{n'=1}^n P_2(n') \quad (\text{B3})$$

2. $Q(n; N \geq 2)$ for Specific Cases

We first consider the case of $F(K) = U(K; A)$. We begin by calculating $P_1(n)$ and $P_2(n)$.

The first kick can take place at any $1 \leq n \leq A$, with equal probability.

$$P_1(n) = \begin{cases} \frac{1}{A}, & 1 \leq n \leq A \\ 0, & \text{otherwise} \end{cases} \quad (\text{B4})$$

From Eq. 17, $P_2(n) = P(K_0 + K_1 = n)$, with $\{K_i\} \leq A$. For $n \leq A + 1$, there are $n - 1$ ways of picking $\{K_i\}$, since choosing K_0 from 1 to $n - 1$ decides K_1 . For $n > A + 1$, the upper limit on $\{K_i\}$ requires that K_0 can only take $(2A - n + 1)$ values from $n - A$ to A .

$$P_2(n) = \frac{1}{A^2} \begin{cases} n - 1, & 2 \leq n \leq A \\ 2A - n + 1, & A < n \leq 2A \\ 0, & \text{otherwise} \end{cases} \quad (\text{B5})$$

If $n \leq A$,

$$\begin{aligned} Q(n; N \geq 2) &= \sum_{n'=1}^n P_2(n') \\ &= \frac{1}{A^2} \sum_{n'=2}^n (n' - 1) \quad (\text{by Eq.18}) \\ Q(n; 1) &= \frac{n(n-1)}{2A^2} \quad (\text{B6}) \end{aligned}$$

If $n > A$

$$\begin{aligned} Q(n; N \geq 2) &= \frac{1}{A^2} \sum_{n'=2}^A (n' - 1) + \frac{1}{A^2} \sum_{n'=A+1}^n (2A - n' + 1) \\ &= \frac{2n - A - 1}{2A} - \frac{(n - A - 1)(n - A)}{2A^2} \quad (\text{B7}) \end{aligned}$$

Putting these together,

$$Q(n; N \geq 2) = \begin{cases} \frac{n(n-1)}{2A^2}, & n \leq A \\ \frac{2n-A-1}{2A} - \frac{(n-A-1)(n-A)}{2A^2}, & A \leq n \leq 2A \\ 1, & n > 2A \end{cases} \quad (\text{B8})$$

Next, we consider $F(K) = P(K; \lambda)$, for which it is straightforward to calculate $P_N(n)$ for any n and N . By construction, more than 1 kick at a time step is not allowed and thus we have

$$P(K; \lambda) \equiv e^{-\lambda} \frac{\lambda^{K-1}}{(K-1)!} \theta(K-1), \quad (\text{B9})$$

where $\theta(x)$ is the Heaviside Step-Function with the convention that $\theta(0) = 1$. Then, we get

$$P_N(n) = \sum_{\{n_j\}}' \prod_{j=1}^N P(K = n_j; \lambda) \quad (\text{B10})$$

where prime indicates that the summation over $\{n_j\}$ is

performed subject to the constraint $\sum_{j=1}^N n_j = n$.

$$\begin{aligned} P_N(n) &= \theta(n-N) \sum_{\{n_j\}}' e^{-N\lambda} \prod_{j=1}^N \frac{\lambda^{n_j-1}}{(n_j-1)!} \\ &= \theta(n-N) e^{-N\lambda} \lambda^{n-N} \sum_{\{n_j\}}' \frac{1}{(n_1-1)! \dots (n_N-1)!} \end{aligned} \quad (\text{B11})$$

Under the redefinition of $n_j - 1 \rightarrow n_j$, such that the condition under the sum becomes $\sum n_j = n - N$, and the multinomial expansion, we have

$$P_N(n) = \theta(n-N) e^{-N\lambda} \frac{(N\lambda)^{n-N}}{(n-N)!} \quad (\text{B12})$$

The actual form of $Q(n; N \geq 2)$ is not particularly useful, and we require just the median of $P_2(n)$, which is known to be $\approx 2\lambda$ for large λ .

Appendix C: $\sigma^2(N)$ for the 2-band coin-toss model

In the 2-band case, the quantity σ^2 has an exact solution in terms of a 4×4 “disorder matrix”, introduced in [57]. We begin by defining $\sigma^2(N)$ using the noisy operators,

$$\sigma^2(N) = \sum_{\substack{\{i_n, j_n\} \\ k_1, k_2}} \langle \psi_0 | i_0 \rangle \langle j_0 | \psi_0 \rangle \left(\prod_{n=1}^N \langle i_{n-1} | F_{k_1}^\dagger | i_n \rangle \langle j_{n-1} | F_{k_1}^T | j_n \rangle \right) \frac{\partial^2}{\partial k_1 \partial k_2} \delta(k_1 - k_2) \quad (\text{C1})$$

$$\begin{aligned} \overline{\langle i_{n-1} | F_{k_1}^\dagger | i_n \rangle \langle j_{n-1} | F_{k_1}^T | j_n \rangle} &= p_k \langle i_{n-1} | F_{k_1}^\dagger(\lambda) | i_n \rangle \langle j_{n-1} | F_{k_1}^T(\lambda) | j_n \rangle \\ &\quad + (1 - p_k) \langle i_{n-1} | F_{k_1}^\dagger(0) | i_n \rangle \langle j_{n-1} | F_{k_1}^T(0) | j_n \rangle. \end{aligned} \quad (\text{C2})$$

One can define the following matrices

$$\begin{aligned} D_1 &:= p_k \left[F_k^\dagger(\lambda) \otimes F_k^T(\lambda) \right] + (1 - p_k) \left[F_k^\dagger(0) \otimes F_k^T(0) \right] \\ D_2 &:= p_k \left[F_k^\dagger(\lambda) \otimes \partial_k (F_k^T(\lambda)) \right] + (1 - p_k) \left[F_k^\dagger(0) \otimes \partial_k (F_k^T(0)) \right] \\ D_3 &:= p_k \left[\partial_k (F_k^\dagger(\lambda)) \otimes F_k^T(\lambda) \right] + (1 - p_k) \left[\partial_k (F_k^\dagger(0)) \otimes F_k^T(0) \right] \\ D_4 &:= p_k \left[\partial_k (F_k^\dagger(\lambda)) \otimes \partial_k (F_k^T(\lambda)) \right] + (1 - p_k) \left[\partial_k (F_k^\dagger(0)) \otimes \partial_k (F_k^T(0)) \right], \end{aligned} \quad (\text{C3})$$

in terms of which one can express $\sigma^2(N)$ as

$$\begin{aligned} \sigma^2(N) &= \\ \frac{1}{L} \sum_{\substack{i_0, j_0 \\ i_N, j_N}} \sum_{n=1}^N \delta_{i_N, j_N} &\left[D_1^{n-1} D_4 D_1^{N-n} + \sum_{m=1}^{n-1} (D_1^{m-1} D_3 D_1^{n-m-1} D_2 D_1^{N-n} + D_1^{m-1} D_2 D_1^{n-m-1} D_3 D_1^{N-n}) \right]_{(i_0, j_0, i_N, j_N)}, \end{aligned} \quad (\text{C4})$$

where the δ_{i_N, j_N} follows from applying $\delta(k_1 - k_2)$ in the discrete limit. Certain recursion relations prove helpful in

reducing the computational complexity of this evaluation

to $\mathcal{O}(N)$. These are

$$\begin{aligned}
 A(N) &= A(N-1)D_1 + D_1^{N-1}D_4; \quad A(0) := 0, \\
 B(N) &= B(N-1)D_1 + \tilde{B}(N-1)D_3; \quad B(1) := 0, \\
 \tilde{B}(N) &= \tilde{B}(N-1)D_1 + D_1^{N-1}D_2; \quad \tilde{B}(0) := 0 \\
 C(N) &= C(N-1)D_1 + \tilde{C}(N-1)D_2; \quad C(1) := 0 \\
 \tilde{C}(N) &= \tilde{C}(N-1)D_1 + D_1^{N-1}D_3; \quad \tilde{C}(0) := 0, \\
 \sigma^2(N) &= \frac{1}{L} \sum_{i,j} [A(N) + B(N) + C(N)]_{i,j}.
 \end{aligned} \tag{C5}$$

Note that the indices in brackets are not the true indices of the 4×4 matrix D . The recipe to switch between the two type of indices – by employing the Kronecker Product – is

$$[D_1^N]_{(i_0, j_0, i_N, j_N)} := [D_1^N]_{2(i_0-1)+j_0, 2(i_N-1)+j_N}. \tag{C6}$$

-
- [1] T. Oka and S. Kitamura, Annual Review of Condensed Matter Physics **10**, 387 (2019).
- [2] D. Basov, R. Averitt, and D. Hsieh, Nature Materials **16**, 1077 (2017).
- [3] M. Bukov, L. D'Alessio, and A. Polkovnikov, Advances in Physics **64**, 139 (2015).
- [4] A. Haldar and A. Das, Annalen der Physik **529**, 1600333 (2017).
- [5] L. Du, X. Zhou, and G. A. Fiete, Phys. Rev. B **95**, 035136 (2017).
- [6] C. M. Dai, W. Wang, and X. X. Yi, Phys. Rev. A **98**, 013635 (2018).
- [7] F. Grossmann, T. Dittrich, P. Jung, and P. Hänggi, Phys. Rev. Lett. **67**, 516 (1991).
- [8] F. Harper, R. Roy, M. S. Rudner, and S. Sondhi, Annual Review of Condensed Matter Physics **11**, 345 (2020).
- [9] M. J. Park, Y. Kim, G. Y. Cho, and S. Lee, Phys. Rev. Lett. **123**, 216803 (2019).
- [10] N. Goldman and J. Dalibard, Phys. Rev. X **4**, 031027 (2014).
- [11] T. Schuster, S. Gazit, J. E. Moore, and N. Y. Yao, Phys. Rev. Lett. **123**, 266803 (2019).
- [12] M. Aidelsburger, M. Atala, M. Lohse, J. T. Barreiro, B. Paredes, and I. Bloch, Phys. Rev. Lett. **111**, 185301 (2013).
- [13] P. Kiefer, F. Hakelberg, M. Wittemer, A. Bermúdez, D. Porras, U. Warring, and T. Schaetz, Phys. Rev. Lett. **123**, 213605 (2019).
- [14] G. Jotzu, M. Messer, and R. D. et. al., Nature **515**, 237 (2014).
- [15] A. Rubio-Abadal, M. Ippoliti, S. Hollerith, D. Wei, J. Rui, S. L. Sondhi, V. Khemani, C. Gross, and I. Bloch, Phys. Rev. X **10**, 021044 (2020).
- [16] T. N. Ikeda and M. Sato, Science Advances **6**, 10.1126/sciadv.abb4019 (2020).
- [17] E. Abrahams, *50 years of Anderson Localization* (World Scientific, 2010).
- [18] R. Nandkishore and D. A. Huse, Annual Review of Condensed Matter Physics **6**, 15 (2015).
- [19] L. Reichl, *The Transition to Chaos: Conservative Classical Systems and Quantum Manifestations* (Springer Science & Business Media, 2004).
- [20] S. Fishman, D. R. Grempel, and R. E. Prange, Phys. Rev. Lett. **49**, 509 (1982).
- [21] F. L. Moore, J. C. Robinson, C. F. Bharucha, B. Sundaram, and M. G. Raizen, Phys. Rev. Lett. **75**, 4598 (1995).
- [22] A. Eckardt, Rev. Mod. Phys. **89**, 011004 (2017).
- [23] B. G. Klappauf, W. H. Oskay, D. A. Steck, and M. G. Raizen, Phys. Rev. Lett. **81**, 1203 (1998).
- [24] E. Ott, T. M. Antonsen, and J. D. Hanson, Phys. Rev. Lett. **53**, 2187 (1984).
- [25] D. Cohen, Phys. Rev. A **44**, 2292 (1991).
- [26] H. Schomerus and E. Lutz, Phys. Rev. A **77**, 062113 (2008).
- [27] S. Sarkar, S. Paul, C. Vishwakarma, S. Kumar, G. Verma, M. Sainath, U. D. Rapol, and M. S. Santhanam, Phys. Rev. Lett. **118**, 174101 (2017).
- [28] D.-L. Deng, S. Ganeshan, X. Li, R. Modak, S. Mukerjee, and J. H. Pixley, Annalen der Physik **529**, 1600399 (2017).
- [29] P. Bordia, H. Lüschen, U. Schneider, M. Knap, and I. Bloch, Nature Physics **13**, 460 (2017).
- [30] S. Ray, A. Ghosh, and S. Sinha, Phys. Rev. E **97**, 010101 (2018).
- [31] S. Xu, X. Li, Y.-T. Hsu, B. Swingle, and S. Das Sarma, Phys. Rev. Research **1**, 032039 (2019).
- [32] L. M. Sieberer, M.-T. Rieder, M. H. Fischer, and I. C. Fulga, Phys. Rev. B **98**, 214301 (2018).
- [33] T. Čadež, R. Mondaini, and P. D. Sacramento, Phys. Rev. B **96**, 144301 (2017).
- [34] S. Aubry and G. André, Ann. Israel Phys. Soc **3**, 18 (1980).
- [35] S. Y. Jitomirskaya, Annals of Mathematics **150**, 1159 (1999).
- [36] G. Roati, C. D'Errico, L. Fallani, M. Fattori, C. Fort, M. Zaccanti, G. Modugno, M. Modugno, and M. Inguscio, Nature **453**, 895 (2008).
- [37] M. Schreiber, P. Hodgman, Sean S. and, H. P. Lüschen, M. H. Fischer, R. Vosk, E. Altman, U. Schneider, and I. Bloch, Science **349**, 842 (2015).
- [38] S. Iyer, V. Oganesyan, G. Refael, and D. A. Huse, Phys. Rev. B **87**, 134202 (2013).
- [39] H. Hiramoto and M. Kohmoto, International Journal of Modern Physics B **06**, 281 (1992).
- [40] H. Hiramoto and S. Abe, Journal of the Physical Society of Japan **57**, 1365 (1988).
- [41] T. Geisel, R. Ketzmerick, and G. Petschel, Phys. Rev. Lett. **66**, 1651 (1991).
- [42] D. R. Hofstadter, Phys. Rev. B **14**, 2239 (1976).
- [43] Z. Zhang, P. Tong, J. Gong, and B. Li, Phys. Rev. Lett. **108**, 070603 (2012).
- [44] P. Qin, C. Yin, and S. Chen,

- Phys. Rev. B **90**, 054303 (2014).
- [45] R. Lima and D. Shepelyansky, Phys. Rev. Lett. **67**, 1377 (1991).
 - [46] R. Artuso, G. Casati, and D. Shepelyansky, Phys. Rev. Lett. **68**, 3826 (1992).
 - [47] R. Artuso, G. Casati, F. Borgonovi, L. Rebuzzini, and I. Guarneri, International Journal of Modern Physics B **08**, 207 (1994).
 - [48] C. Sanderson and R. Curtin, Journal of Open Source Software **1**, 26 (2016).
 - [49] C. Sanderson and R. Curtin, in *International Congress on Mathematical Software* (Springer, 2018) pp. 422–430.
 - [50] W. H. Zurek, Decoherence and the transition from quantum to classical — revisited, in *Quantum Decoherence: Poincaré Seminar 2005*, edited by B. Duplantier, J.-M. Raimond, and V. Rivasseau (Birkhäuser Basel, Basel, 2007) pp. 1–31.
 - [51] D. Cohen, Phys. Rev. Lett. **67**, 1945 (1991).
 - [52] J. T. Chalker, T. S. Pickles, and P. Shukla, Phys. Rev. B **82**, 104209 (2010).
 - [53] L. Ge, Ann. Phys. (Berlin) **529**, 1600182 (2017).
 - [54] T. Mizoguchi and M. Udagawa, Phys. Rev. B **99**, 235118 (2019).
 - [55] P. Markos and C. M. Soukoulis, *Wave propagation: from electrons to photonic crystals and left-handed materials* (Princeton University Press, 2008).
 - [56] S. Gopalakrishnan, K. R. Islam, and M. Knap, Phys. Rev. Lett. **119**, 046601 (2017).
 - [57] U. Bhattacharya, S. Maity, U. Banik, and A. Dutta, Phys. Rev. B **97**, 184308 (2018).